Supplementary Information

Zwitterion-Engineered Covalent Organic Frameworks Achieving Record Proton Conductivity for High-Performance Proton Batteries

Guo-Qin Zhang, [a†] *Hao-Yu Li,* [a†] *Si-Liu Wang,* [a] *Qi-Chao Wang,* [a] *Qiao Qiao,* [a] *Hong-Bin Luo,** [a] *Yangyang Liu,* [b] *Xiao-Ming Ren** [a,c]

[a] State Key Laboratory of Materials-Oriented Chemical Engineering and School of Chemistry and Molecular Engineering, Nanjing Tech University, Nanjing 211816, P.R. China

[b] Department of Chemistry and Biochemistry, California State University, Los Angeles, 5151 State University Drive, Los Angeles, CA 90032, USA

[c] State Key Laboratory of Coordination Chemistry, Nanjing University, Nanjing 210023, P. R. China

[†] These authors contributed equally to this work.

[*]Correspondence should be addressed to H. -B. L (hbluo@njtech.edu.cn); X. M. R (xmren@njtech.edu.cn)

Contents

Supplementary Text……...……..…..3

Supplementary Figures……..7

Supplementary Table.……..……13

References……....14

Supplementary Text

1. Chemicals and materials

All chemicals were of analytical grade and used as received without additional purification. 1,2,4,5-Tetracyanobenzene (TCNB, 98%) was supplied by Anhui Zesheng Technology Co., Ltd. Ammonium chloride (NH_4Cl, ≥99.5%) and glycerol (≥99.0%) were obtained from Xilong Scientific Reagent Co., Ltd. Sulfuric acid (H_2SO_4, 95.0–98.0%) and ethanol (≥99.7%) were sourced from Sinopharm Chemical Reagent Co., Ltd., while methanesulfonic acid (CH_3SO_3H, 99.0%) was provided by J&K Scientific Ltd. Vanadium pentoxide (V_2O_5, 99.5%), nitric acid (HNO_3, ≥99.0%), and polytetrafluoroethylene dispersion (PTFE, 60 wt%) were purchased from Shanghai Aladdin Biochemical Technology Co., Ltd. 1-Methyl-2-pyrrolidone (NMP, 98.0%) was also sourced from Aladdin. Hydrochloric acid (HCl, 36.0~38.0%), potassium ferricyanide ($K_3Fe(CN)_6$, ≥99.0%), hydrazine hydrate ($N_2H_4·H_2O$, ≥80.0%), and acetonitrile (CH_3CN, ≥99.5%) were acquired from Shanghai Lingfeng Chemical Reagent Co., Ltd. Ammonium molybdate tetrahydrate ($(NH_4)_6Mo_7O_{24}·4H_2O$, ≥99.0%) was obtained from KeHua Research Institute. Carbon black (MJS-SP-20230923) was purchased from Nanjing Modges Energy Technology Co., Ltd. Lastly, 1,3-propanesulfonate (1,3-PS, 99%) was acquired from Shanghai Macklin Biochemical Co., Ltd.

2. Preparation of Zwitterion-Functionalized pcCOF

pcCOF was synthesized according to a previously reported procedure.[1] pcCOF was prepared by ball milling 300 mg of TCNB and 200 mg of NH_4Cl at 1600 rpm for 1 h. The mixture was placed in a combustion boat and heated at 220 °C for 12 h in a tube furnace. The product washed with DI water and ethanol and dried at 70 °C under vacuum for 24 h.

3. Preparation of Zwitterion-Functionalized Z-pcCOF

Zwitterion-functionalized Z-pcCOF was obtained via a ring-opening reaction between pcCOF and 1,3-propane sultone (1,3-PS). Specifically, pcCOF (0.5 g) was dispersed in 75 mL of acetonitrile and stirred at 85 °C under a nitrogen atmosphere. A solution of 1,3-PS (2.5 g) in 12.5 mL of acetonitrile was added dropwise over 30 min. The resulting mixture was maintained at 85 °C with continuous stirring for 48 h. After cooling to room temperature, the product was washed repeatedly with acetone, acetonitrile, and ethanol to thoroughly remove any unreacted 1,3-PS. The final solid was collected and dried under vacuum at 60 °C for 24 h, affording the zwitterion-functionalized product Z-pcCOF as a fine powder.

4. Preparation of MeSA@Z-pcCOF-X (X = 10, 20, 30, 40, 50, X represents the mass percentage of MeSA)

A series of methanesulfonic acid (MeSA)-doped Z-pcCOF composites, denoted as MeSA@Z-pcCOF-X (X = 0, 10, 20, 30, 40, 50), were prepared by mechanically blending Z-pcCOF with varying weight percentages of MeSA (0 wt%, 10 wt%, 20 wt%, 30 wt%, 40 wt%, and 50 wt%). The doping process was carried out using a planetary ball mill at 1600 rpm for 60 minutes. As the MeSA content increased, the resulting materials exhibited gradual changes in physical properties. Notably, at 50 wt% MeSA, the product exhibited a plastic, quasi-solid-state behavior. Therefore, the sample with 40 wt% doping (MeSA@Z-pcCOF-40) was selected as the highest doping level with retained powder form and considered optimal for further characterization and application.

5. Preparation of MeSA@pcCOF-X (X = 40, 60, X represents the mass percentage of MeSA)

MeSA@pcCOF-X composites (X = 40, 60) were prepared by mechanically blending pcCOF with MeSA at different weight ratios. Specifically, 100 mg of pcCOF was mixed with 101.01 μL and 157.13 μL of MeSA for the 40 wt% and 60 wt% samples, respectively. The mixtures were ground using a planetary ball mill at 1600 rpm for 1 h to yield homogeneous composite powders. MeSA@pcCOF-60 is the product with the highest MeSA doping level among the pcCOF-based composites.

6. Preparation of Z-pcCOF@MeSA-40/PTFE electrolyte membrane

The MeSA@Z-pcCOF-40 composite, which possesses the highest doping level while maintaining powder form, was selected for solid-state electrolyte membrane fabrication. MeSA@Z-pcCOF-40 was thoroughly mixed with 4 wt% PTFE and ground to ensure uniform dispersion. The mixture was then roll-pressed using a roller press to form a uniform, flexible membrane with consistent thickness, denoted as the MeSA@Z-pcCOF-40/PTFE solid-state electrolyte membrane (~100 μm thick).

7. Preparation of cathode/solid electrolyte/anode sandwich solid state proton batteries

The H-VHCF and MoO_3 electrodes were synthesized according to previously reported methods.[2-4] The solid-state proton batteries were fabricated in a sandwich-type configuration comprising an H-VHCF cathode, a MoO_3 anode, and a solid-state electrolyte membrane. To prepare the H-VHCF cathode membrane, H-VHCF powder (70 wt%), carbon black (20 wt%), and PTFE dispersion (10 wt%, 60 wt% in H_2O) were thoroughly mixed in NMP to form a uniform slurry. The resulting dough-like mixture was roll-pressed into a freestanding membrane, followed by vacuum drying at 60 °C for 12 h. The dried membrane was then cut into 0.5 × 0.5 cm^2 pieces and pressed onto titanium mesh using a roller press to serve as the cathode, with a total mass of 1.5 mg. The MoO_3 anode membrane was prepared using a similar

procedure, except ethanol was used as the dispersing solvent instead of NMP. MoO_3, carbon black, and PTFE were also mixed in a weight ratio of 70:20:10, followed by the same pressing and drying steps to form the anode electrode. The electrode has a total mass of 1.7 mg and a geometric area of 0.5 × 0.5 cm^2. The MeSA@Z-pcCOF-40/PTFE solid-state electrolyte membrane was then cut into pieces slightly larger than 0.5 × 0.5 cm^2. Battery assembly was completed by stacking the H-VHCF cathode, electrolyte membrane, and MoO_3 anode in sequence. Care was taken to avoid direct contact between the electrodes to prevent short-circuiting.

An aluminum-plastic film was used as the outer packaging for the pouch cell. The cathode and anode electrodes were respectively connected to an aluminum tab and a nickel tab. The cell was then vacuum-sealed with heat to form a compact 0.5 × 0.5 cm^2 pouch-type solid-state proton battery. For the fabrication of series-connected pouch cells, the same aluminum–plastic film packaging was employed. Internally, three individual proton cells were assembled in series by connecting the cathode of one cell to the anode of the next (i.e., cathode-to-anode configuration). After assembling the three-cell series unit, the H-VHCF cathode at one end and the MoO_3 anode at the other end were respectively connected to aluminum and nickel tabs. The assembled structure was then vacuum-sealed with heat, yielding a miniaturized, high-voltage, triple-cell series pouch battery.

8. Characterization methods

Powder X-ray diffraction (PXRD) patterns were collected on a Rigaku MiniFlex600 diffractometer with Cu Kα radiation (λ = 1.5404 Å) as the X-ray source. The chemical structures and functional groups of the samples were examined by Fourier-transform infrared (FT-IR) spectroscopy using a Nicolet iS5 spectrometer. X-ray photoelectron spectroscopy (XPS) was carried out on a PHI 5000 VersaProbe system with Al K$\underline{\alpha}$ excitation, and the binding energy of Ag $3d_{5/2}$ was used for calibration. Ultraviolet-visible (UV-Vis) absorption spectra were recorded using a PerkinElmer Lambda 1050+ 2D UV-Vis-NIR spectrophotometer. Morphological features and elemental distributions of the samples were investigated by scanning electron microscopy (SEM) and energy-dispersive X-ray spectroscopy (EDS) using a Quanta FEG-250 field-emission microscope. High-resolution transmission electron microscopy (HRTEM) images were obtained with a FEI Talos F200X G2 instrument. Thermal stability was assessed through thermogravimetric analysis (TGA) under both air and nitrogen atmospheres from 298 K to 1000 K at a heating rate of 10 $K \cdot min^{-1}$, using a DTA-TGA 2960 thermal analyzer. Elemental compositions (C, H, N, S) were determined using a Vario MICRO cube elemental analyzer. Electrochemical impedance spectroscopy (EIS) was performed on a Gamry

Reference 600+ electrochemical workstation using a 5 mV AC perturbation over a frequency range of 1 Hz to 5 MHz in a standard three-electrode configuration. Linear sweep voltammetry (LSV) measurements were conducted in 1 M H_2SO_4 solution using a titanium/sample working electrode, a platinum counter electrode, and a saturated calomel electrode (SCE) as reference. Galvanostatic charge-discharge (GCD) tests for the solid-state proton batteries were carried out using a LAND CT2001 battery testing system in a voltage range of 0.1~1.6 V. Water contact angle measurements were performed using a contact angle goniometer (DSA25S) to evaluate the surface wettability of the solid-state electrolyte membranes.

9. Testing methods

Proton conductivity (σ_p) measurements were carried out using a Gamry Reference 600+ electrochemical workstation configured in a standard three-electrode setup. Approximately 100 mg of the powdered sample was loaded into a polypropylene (PPL) ring with an inner diameter of 10 mm. Gold electrodes were placed at both ends of the sample, and the entire assembly was compressed between two titanium alloy electrodes under a pressure of 10 MPa, forming a pellet with a thickness of approximately 2 mm. The compacted sample was then sealed and subjected to EIS.

The conductivity was calculated using the equation:

$$\sigma_P = L/RS,$$

where R represents the measured resistance, L is the thickness of the pellet, and S denotes the cross-sectional area. The temperature-dependent proton conductivity was further analyzed using the Arrhenius equation:

$$\sigma_P = \sigma_0 \exp\left(\frac{-E_a}{k_B T}\right),$$

where σ_0 is the pre-exponential factor, E_a is the activation energy, k_B is the Boltzmann constant, and T is the absolute temperature.

For battery performance evaluation, both the assembled sandwich-type solid-state proton batteries and three-electrode configuration cells were rested for 1 h prior to testing. Galvanostatic charge-discharge (GCD) tests were performed using a LAND CT2001 battery testing system, operated at controlled current densities and voltage cutoffs inside a thermostatic oven set to 25 °C. Based on the mass of the active material, specific capacity and Coulombic efficiency were calculated for each charge-discharge cycle to evaluate electrochemical performance and cycling stability.

Supplementary Figures

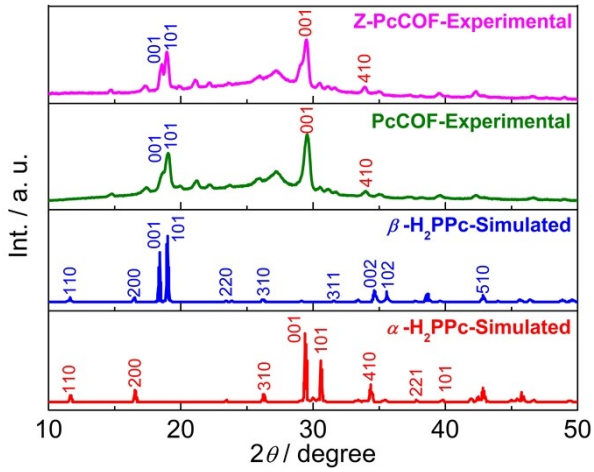

Fig. S1 PXRD patterns of pc-COF and Z-pcCOF. The characteristic peaks show good agreement, and similar PXRD analyses have been reported.[5]

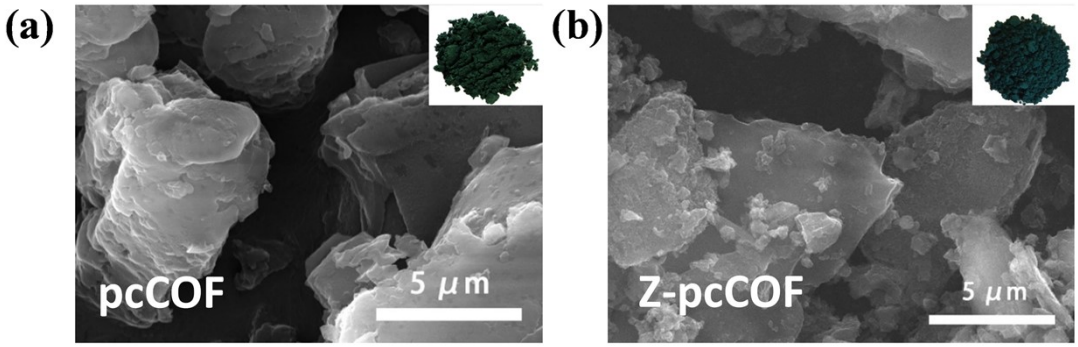

Fig. S2 SEM images of (a) pcCOF and (b) Z-pcCOF (the illustration is optical photograph of the sample powders).

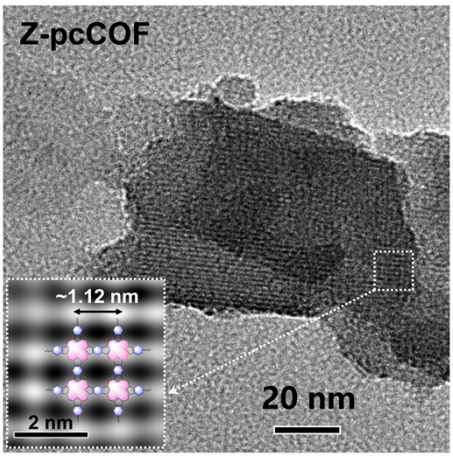

Fig. S3 HRTEM image of Z-pcCOF.

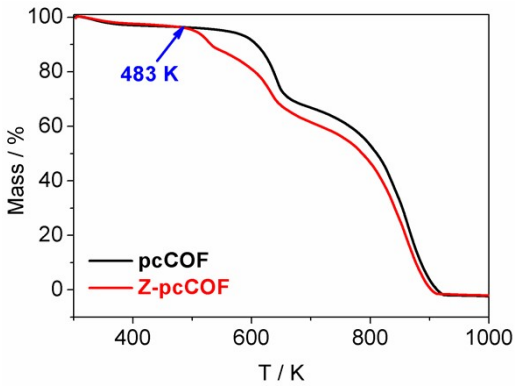

Fig. S4 TG curves of pcCOF and Z-pcCOF.

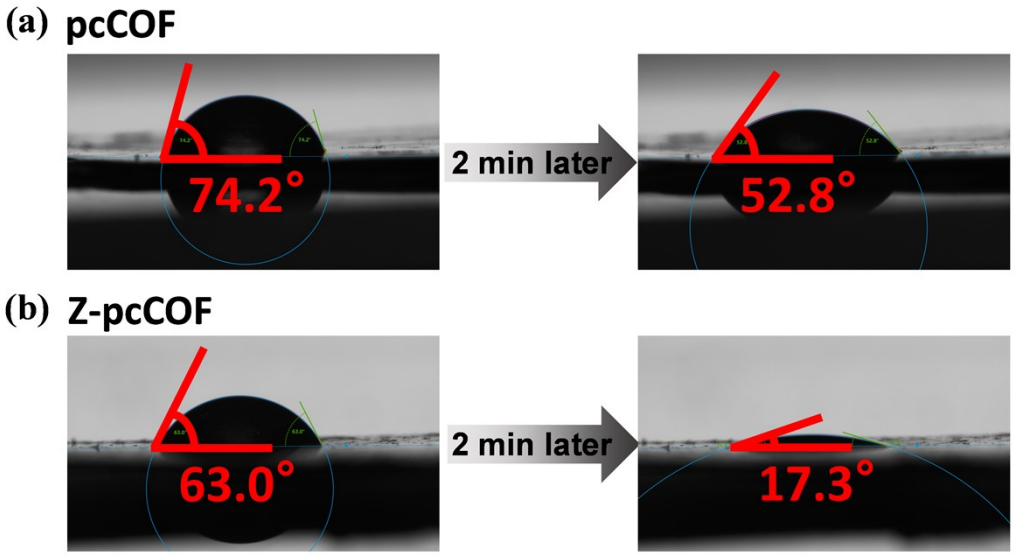

Fig. S5 Water contact angle measurements of (a) pcCOF and (b) Z-pcCOF.

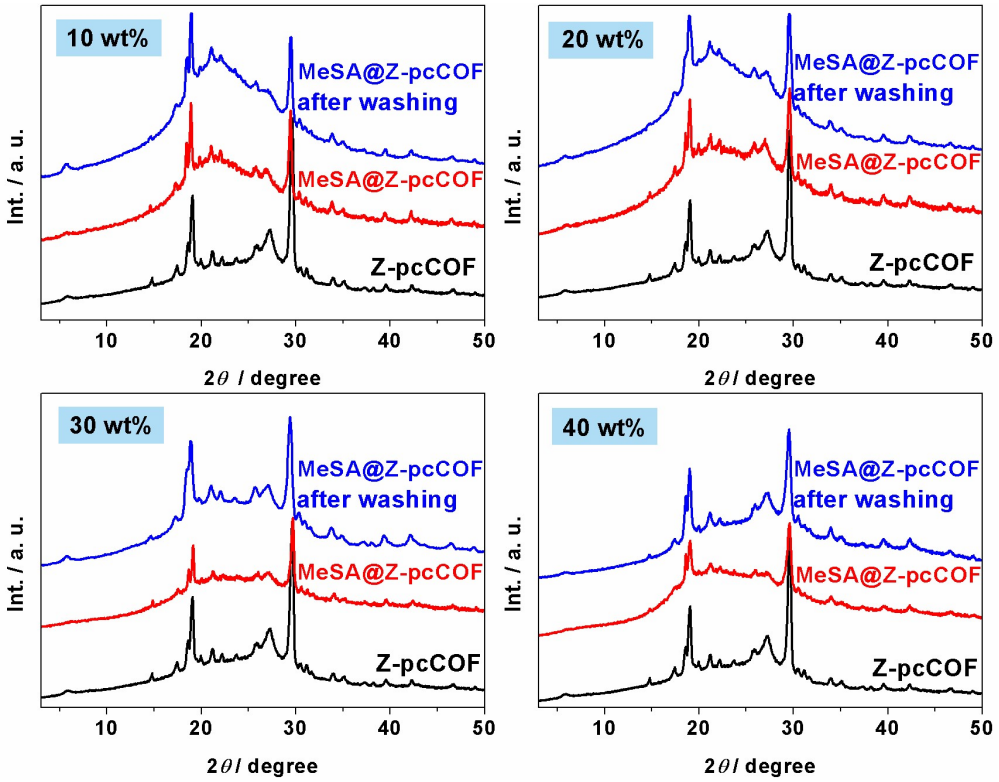

Fig. S6 PXRD patterns of Z-pcCOF, MeSA@Z-pcCOF with different MeSA contents, and Z-pcCOF from which MeSA molecules have been washed away using deionized water and ethanol.

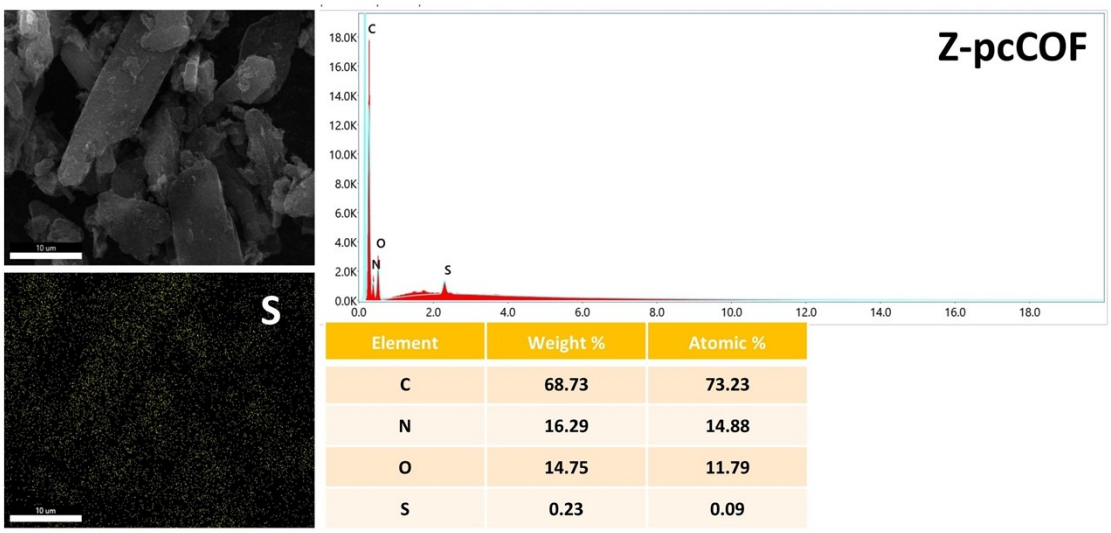

Element	Weight %	Atomic %
C	68.73	73.23
N	16.29	14.88
O	14.75	11.79
S	0.23	0.09

Fig. S7 SEM image and its corresponding EDS mapping of Z-pcCOF.

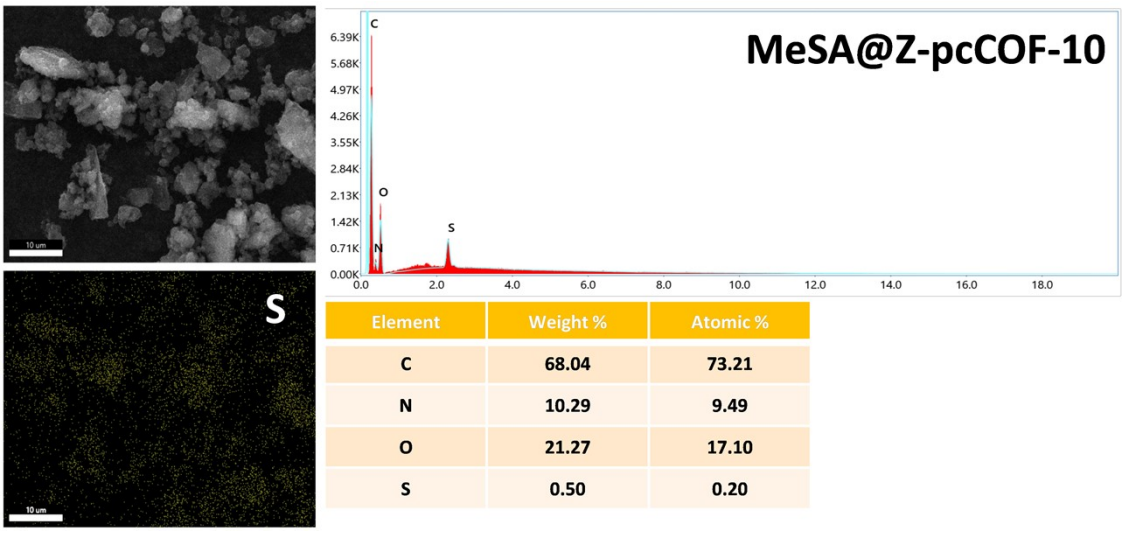

Element	Weight %	Atomic %
C	68.04	73.21
N	10.29	9.49
O	21.27	17.10
S	0.50	0.20

Fig. S8 SEM image and its corresponding EDS mapping of MeSA@Z-pcCOF-10.

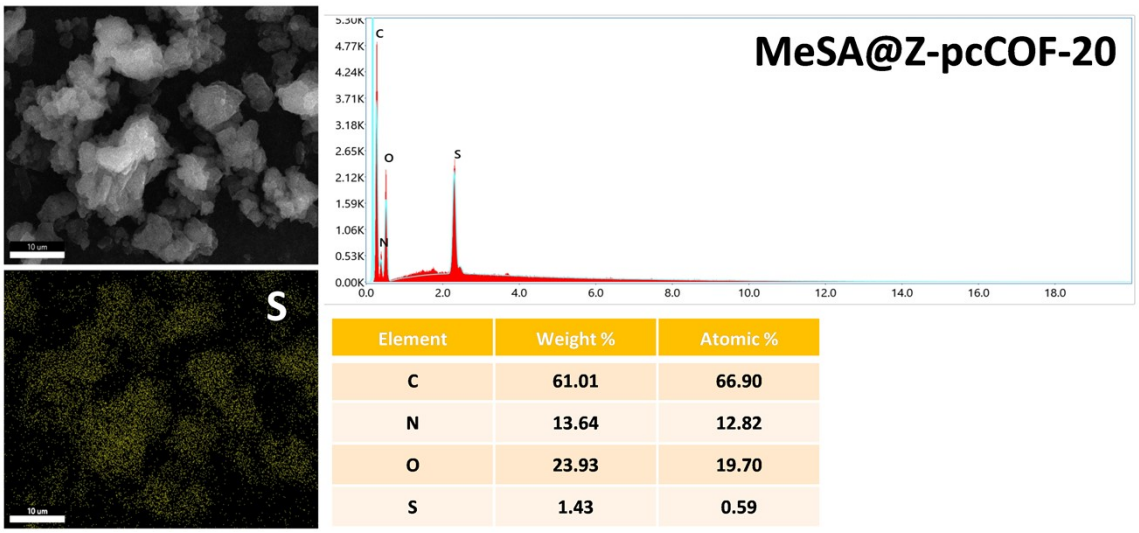

Element	Weight %	Atomic %
C	61.01	66.90
N	13.64	12.82
O	23.93	19.70
S	1.43	0.59

Fig. S9 SEM image and its corresponding EDS mapping of MeSA@Z-pcCOF-30.

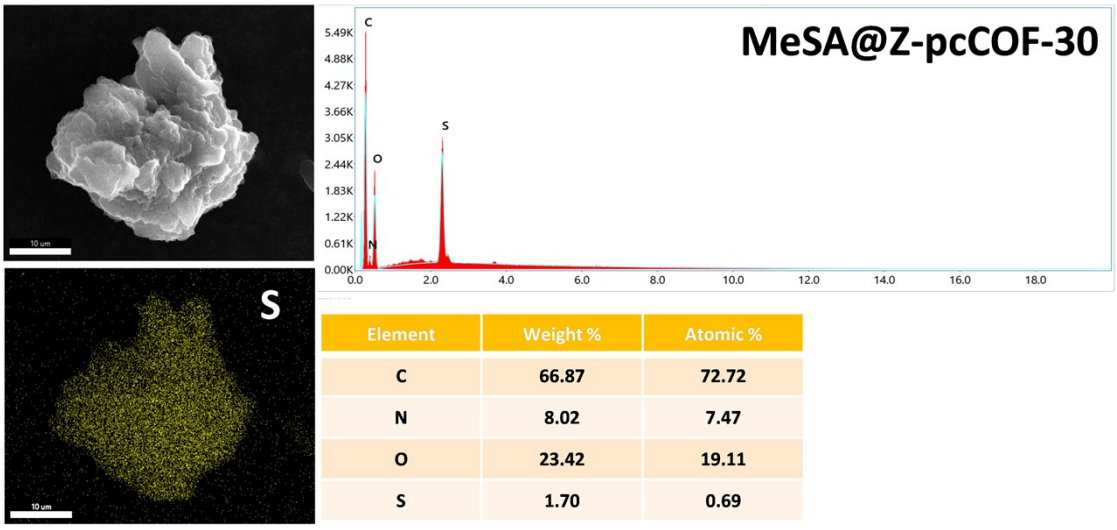

Element	Weight %	Atomic %
C	66.87	72.72
N	8.02	7.47
O	23.42	19.11
S	1.70	0.69

Fig. S10 SEM image and its corresponding EDS mapping of MeSA@Z-pcCOF-30.

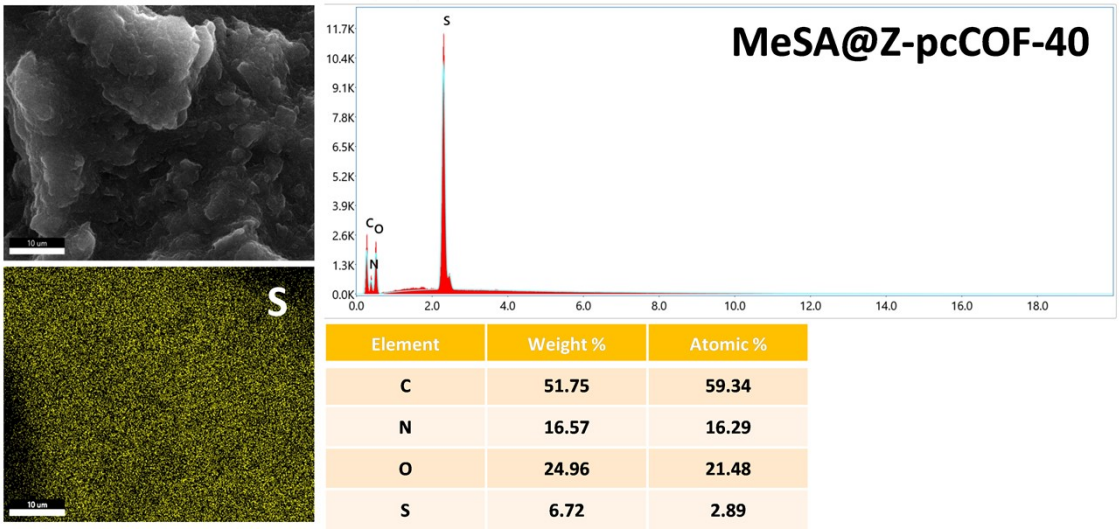

Element	Weight %	Atomic %
C	51.75	59.34
N	16.57	16.29
O	24.96	21.48
S	6.72	2.89

Fig. S11 SEM image and its corresponding EDS mapping of MeSA@Z-pcCOF-40.

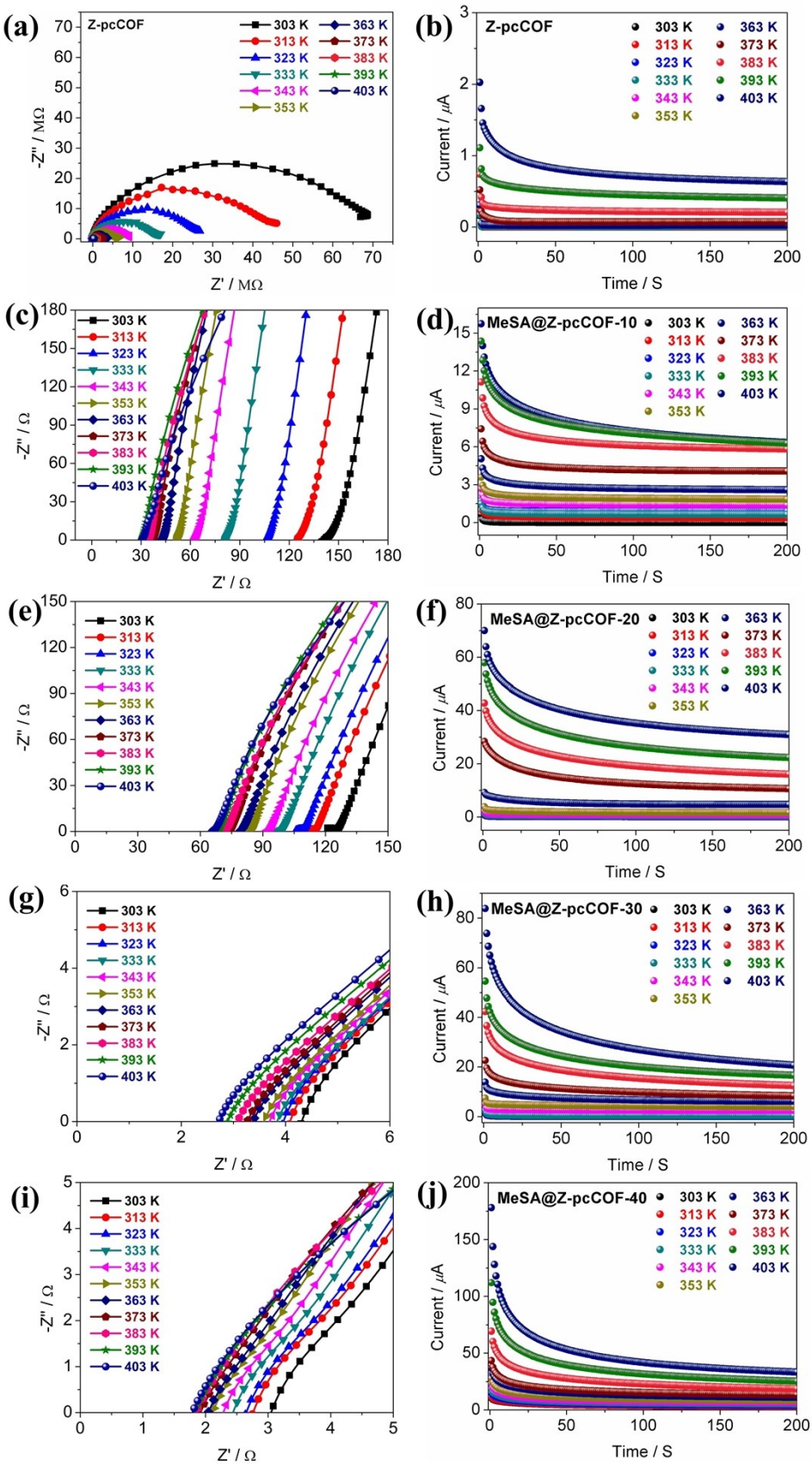

Fig. S12 Nyquist plots and current variation curve against time under different temperatures of (a, b) Z-pcCOF, (c, d) MeSA@Z-pcCOF-10, (e, f) MeSA@Z-pcCOF-20, (g, h) MeSA@Z-pcCOF-30, (i, j) MeSA@Z-pcCOF-40.

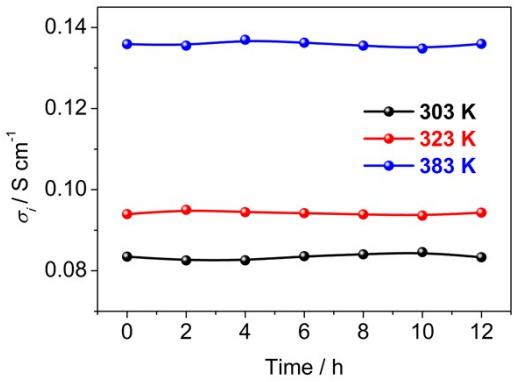

Fig. S13 Proton-conducting long-term stability of MeSA@Z-pcCOF-40.

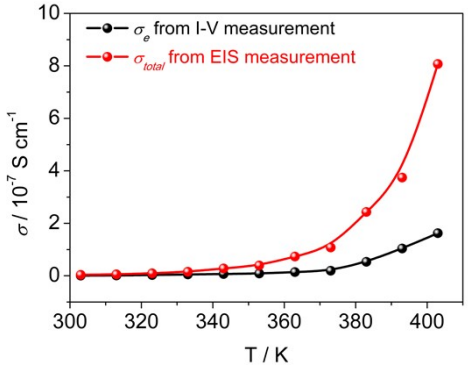

Fig. S14 The temperature-dependent ionic conductivity and total conductivity plots of Z-pcCOF.

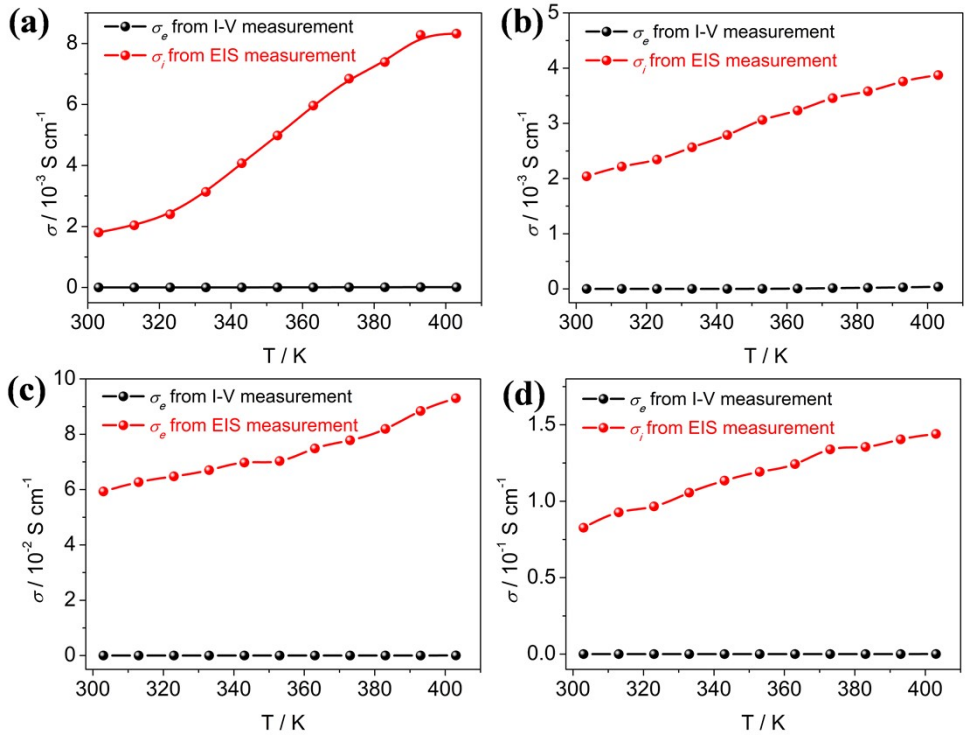

Fig. S15 The temperature-dependent ionic conductivity and electronic conductivity plots of (a) MeSA@Z-pcCOF-10, (b) MeSA@Z-pcCOF-20, (c) MeSA@Z-pcCOF-30 and (d) MeSA@Z-pcCOF-40.

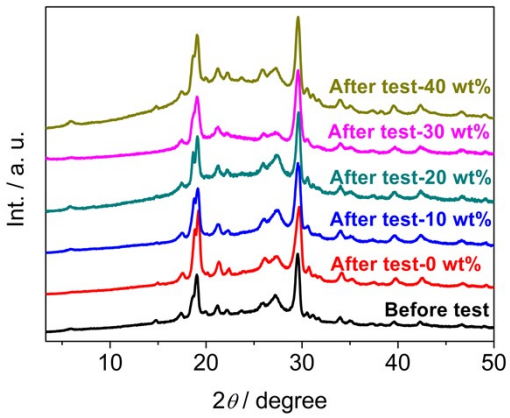

Fig. S16 PXRD patterns of Z-pcCOF and MeSA@Z-pcCOF sample before and after EIS testing.

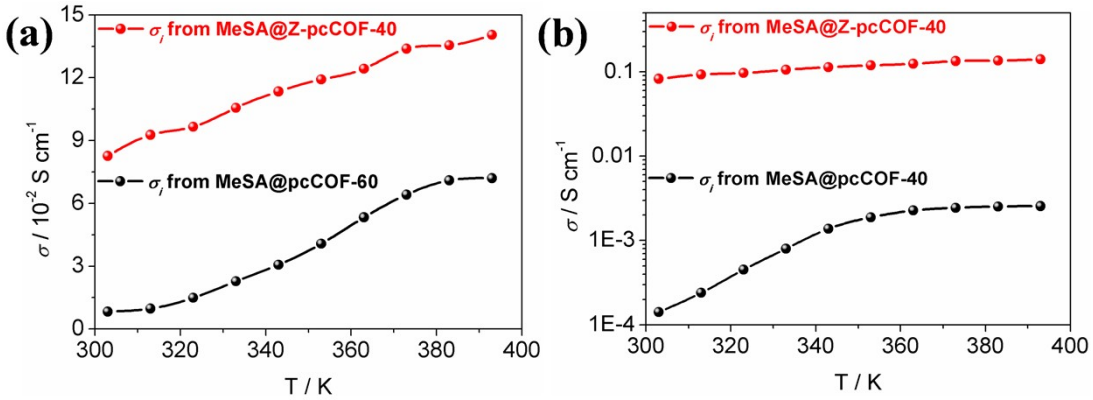

Fig. S17 (a) Proton conductivity comparison between MSA@H_2PPc-60 and MSA@Z-H_2PPc-40 at their respective optimal acid doping levels. (b) Proton conductivity comparison of MSA@H_2PPc-40 and MSA@Z-H_2PPc-40 at identical acid doping levels.

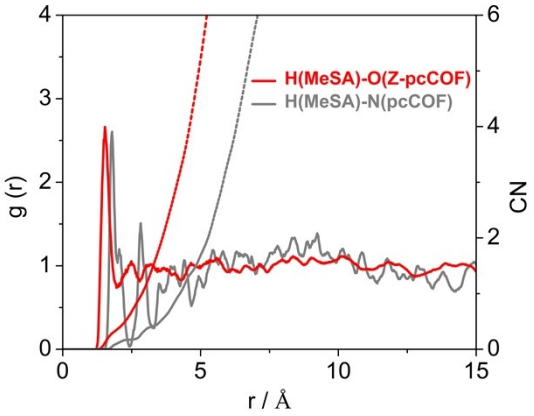

Fig. S18 Radial distribution functions (RDF) of H(MeSA)-O(Z-pcCOF) and H(PA)-O(pcCOF), along with the coordination numbers (CN).

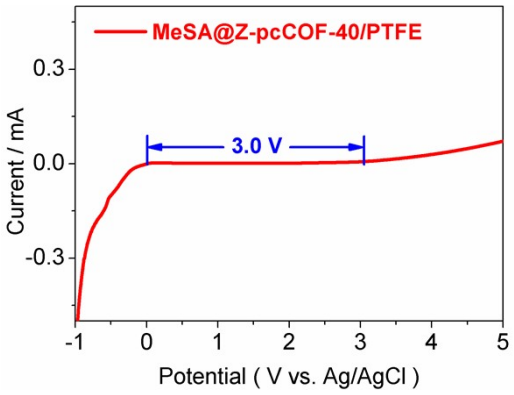

Fig. S19 LSV curve of MSA@Z-H_2PPc-40/PTFE composite showing the electrochemical stability window.

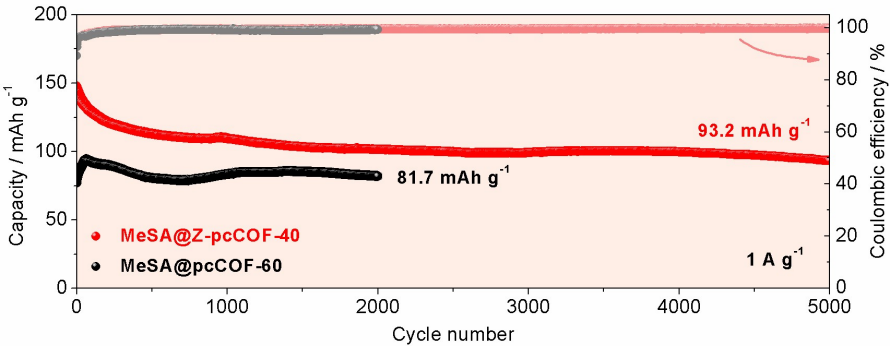

Fig. S20 Comparison of the cycling performance of proton batteries with MSA@Z-H_2PPc-40 and MSA@H_2PPc-60-based solid-state electrolytes.

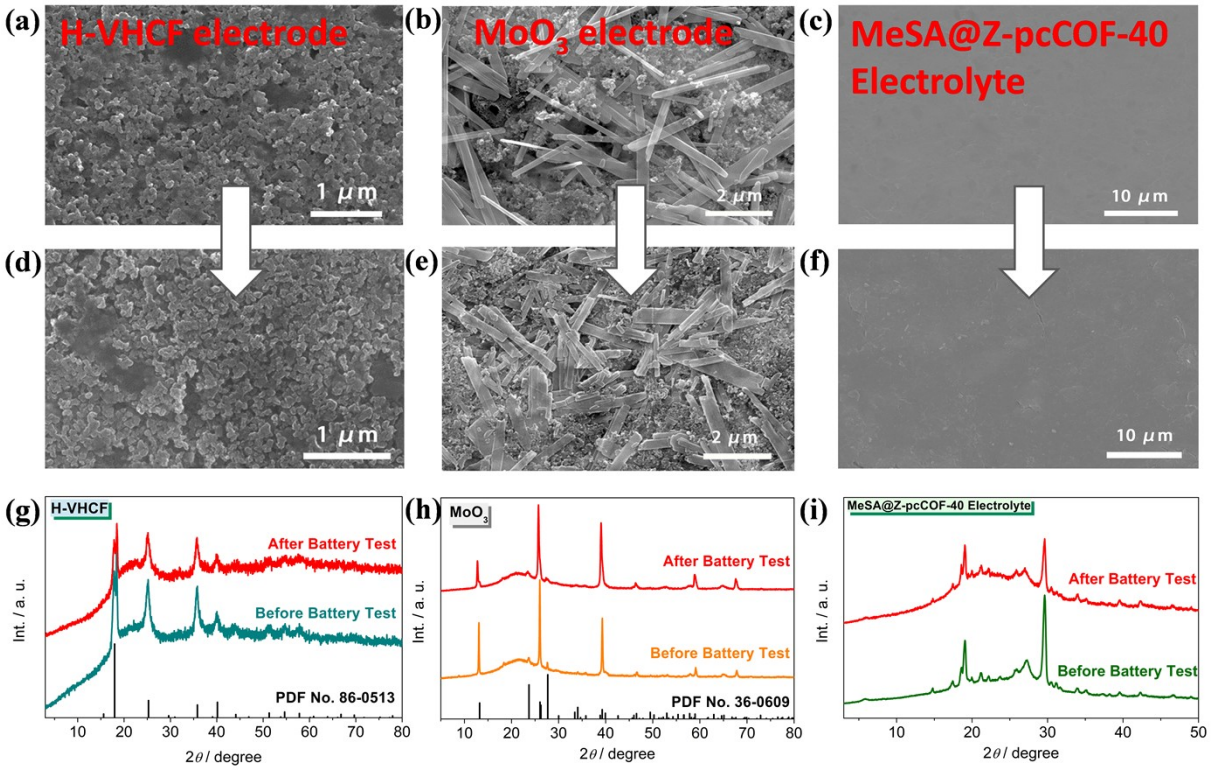

Fig. S21 SEM images and PXRD patterns of the H-VHCF cathode, MoO_3 anode, and MeSA@Z-pcCOF-40 electrolyte before and after proton battery testing.

Supplementary Table

Table S1 The elemental analyses of Z-pcCOF and MeSA@Z-pcCOF-X (X = 10, 20, 30, 40).

Materials	N%	C%	H%	S%	C/N	S/N
Z-pcCOF	20.70	50.73	3.180	5.13	2.45	0.25
MeSA@Z-pcCOF-10	17.57	47.11	3.137	4.499	2.68	0.26
MeSA@Z-pcCOF-20	14.85	40.44	3.464	7.382	2.72	0.50
MeSA@Z-pcCOF-30	11.49	33.34	3.569	9.202	2.90	0.80
MeSA@Z-pcCOF-40	10.90	29.67	4.024	11.251	2.72	1.03

Table S2 The proton conductivity at room temperature and activation energy for samples with the same acid doping content and the highest acid doping content.

Materials	σ / S cm^{-1}	E_a / eV
MeSA@Z-pcCOF-40	8.26×10^{-2}	0.09
MeSA@pcCOF-60	8.25×10^{-3}	0.30
MeSA@pcCOF-40	1.42×10^{-4}	0.37

Table S3 The proton conduction of MeSA@Z-pcCOF-40 in comparison with other COF-based proton-conducting materials under unhumidified condition.

Materials	**σ / S cm^{-1}**	**T / K**	**Ref.**
COF-3@PA-30	1.4	423	[6]
	3.80×10^{-1}	343	
H_3PO_4@TPB-DABI-COF	1.52×10^{-1}	433	[7]
	1.39×10^{-1}	423	
	1.22×10^{-1}	413	
	1.09×10^{-1}	403	
	9.71×10^{-2}	393	
	8.59×10^{-2}	383	
	7.37×10^{-2}	373	
MeSA@Z-pcCOF-40	1.44×10^{-1}	403	**This work**
	1.40×10^{-1}	393	
	1.36×10^{-1}	383	
	1.34×10^{-1}	373	
	1.24×10^{-1}	363	
	1.19×10^{-1}	353	

	1.13×10^{-1}	343	
	1.06×10^{-1}	333	
	9.66×10^{-2}	323	
	9.27×10^{-2}	313	
	8.26×10^{-2}	303	
COF-F6-H	4.20×10^{-2}	413	8
	2.60×10^{-2}	353	
	1.40×10^{-2}	313	
PA@EB-COF	2.77×10^{-2}	453	9
	9.66×10^{-3}	433	
	6.63×10^{-3}	413	
	4.96×10^{-3}	393	
	3.07×10^{-3}	373	
	1.60×10^{-3}	353	
H_3PO_4@NKCOF-54	2.33×10^{-2}	433	10
	1.88×10^{-2}	413	
	1.44×10^{-2}	393	
	8.89×10^{-3}	373	
	5.40×10^{-3}	353	
MeSA@H_2PPc-60	7.20×10^{-2}	393	1
	5.33×10^{-2}	363	
	8.25×10^{-3}	303	
PASPCOF-0.75	3.6×10^{-3}	403	11
	1.4×10^{-3}	353	
	1.0×10^{-3}	303	
C6-[dema]HSO_4-1.0	2.84×10^{-3}	413	12
	1.19×10^{-3}	373	
	1.20×10^{-4}	313	

References

1 G. Q. Zhang, B. Liu, H. Y. Li, S. P. Ye, S. Zuo, Q. Qiao, G. P. Liu, H. B. Luo and X. M. Ren, *Small*, 2025, **21**, 2505839.

2 X. C. Peng, H. C. Guo, W. H. Ren, Z. Su and C. Zhao, *Chem. Commun*., 2020, **56**, 11803-11806.

3 X. Y. Dong, Z. W. Li, D. R. Luo, K. S. Huang, H. Dou and X. G. Zhang, *Adv. Funct. Mater.*, 2023, **33**, 2210473.

4 H. Dong, L. L. Wang, Z. R. Feng, J. Song, Q. Qiao, Y. P. Wu and X. M. Ren, *J. Mater. Chem. C*, 2023, **11**, 13113-13119.

5 W. Y. Wang, C. Yang, M. C. Chen, D. T. Han, W. T. Qi, R. Ling, S. S. Xu and G. Q. Liu, *Appl. Catal. B* 2021, **299**, 120637.

6 Q. Q. Yang, X. Y. Li, C. S. Xie, N. Liu, J. J. Yang, Z. H. Kong, Z. X. Kang, R. M. Wang, X. Y. Li and D. F. Sun, *Nano Res.*, 2023, **16**, 10946-10955.

7 J. Li, J. Wang, Z. Z. Wu, S. S. Tao and D. L. Jiang, *Angew. Chem. Int. Ed*., 2021, **60**, 12918-12923.

8 X. W. Wu, Y. L. Hong, B. Q. Xu, Y. Nishiyama, W. Jiang, J. W. Zhu, G. Zhang, S. Kitagawa and S. Horike, *J. Am. Chem. Soc.*, 2020, **142**, 14357-14364.

9 S. H. Chen, Y. Wu, Y. Zhang, W. X. Zhang, Y. Fu, W. B. Huang, Y. Tong and H. P. Ma, *J. Mater. Chem. A*., 2020, **8**, 13702-13709.

10 L. Q. Hao, S. P. Jia, X. L. Qiao, E. Lin, Y. Yang, Y. Chen, P. Cheng and Z. J. Zhang, *Angew. Chem. Int. Ed*., 2023, **62**, e202217240.

11 K. Divya, Q. Q. Liu, R. Murali, M. R. Asghar, H. Y. Liu, W. Q. Zhang, Q. Xu, J. W. Ren and H. N. Su, *Appl. Surf. Sci*., 2025, **681**, 161544.

12 X. W. Wu, Z. Y. Liu, H. Guo, Y. L. Hong, B. Q. Xu, K. Zhang, Y. Nishiyama, W. Jiang, S. Horike and S. Kitagawa, *ACS Appl. Mater. Interfaces*., 2021, **13**, 37172-37178.